Case Studies in Construction Materials 19 (2023) e02266

Contents lists available at ScienceDirect

Case Studies in Construction Materials

journal homepage: www.elsevier.com/locate/cscm

Effect of using sugarcane leaf ash and granite dust as partial replacements for cement on characteristics of ultra-high performance concrete

Ibrahim Y. Hakeem [a], Mohamed Amin [b,c], Ibrahim Saad Agwa [b,d,*], Mostafa S. Rizk [d], Mohammad Farouk Abdelmagied [e]

[a] Department of Civil Engineering, College of Engineering, Najran University, Najran, Saudi Arabia
[b] Civil and Architectural Constructions Department, Faculty of Technology and Education, Suez University, Egypt
[c] Civil Engineering Department, Mansoura High Institute for Engineering and Technology, Mansoura, Egypt
[d] Department of Civil Engineering, El-Arish High Institute for Engineering and Technology, El-Arish, North Sinai, Egypt
[e] Civil Engineering Department, Benha Faculty of Engineering, Benha University, Benha, Egypt

ARTICLE INFO

Keywords:
Granite dust
Mechanical characteristics
Recycled fine aggregate
Sugarcane leaf ash
Ultra-high performance concrete

ABSTRACT

A significant quantity of cement is necessary for the production of ultra-high-performance concrete (UHPC). However, some environmental issues are associated with cement production. The worldwide agricultural growth increases ash from agricultural waste (AW). Furthermore, industrial waste (IW) generated throughout the stone-cutting and processing has increased due to the growing demand for granite stone in construction. This research conducted a unique study that involved comparing the use of sugarcane leaf ash (SLA) as AW and granite dust (GD) as IW as partial substitutes for cement in the production of eco-friendly UHPC. The effect of employing SLA and GD with replacement ratios ranging from 20% to 50% on the mechanical and transport properties of UHPC was studied. In addition, this research investigated the effectiveness of partial replacement of natural fine aggregate (NFA) by recycled fine aggregate (RFA) with ratios ranging from 25% to 100% on the UHPC qualities. Moreover, the effect of elevated temperatures on the UHPC and the microstructural examination were investigated. Results demonstrated that the optimum replacement ratio of SLA or GD from cement was 20%, showing the best mechanical characteristics of the UHPC. For example, after 28 days of casting, the compressive strength increased by 12.16% and 8.44% when SLA and GD were added to the UHPC mix, respectively. Additionally, the 25% replacement ratio of RFA from NFA presented the best mechanical and transport properties of the UHPC. The mixes containing SLA positively affected the UHPC higher than those containing GD.

1. Introduction

The demand for construction supplies has significantly increased due to the world's population growth and economic expansion. The construction industry heavily relies on concrete [1]. This situation results in a yearly increase in the need for cement. However, environmental issues are associated with cement, including significant atmospheric carbon dioxide emissions and non-renewable

* Corresponding author at: Civil and Architectural Constructions Department, Faculty of Technology and Education, Suez University, Egypt.
E-mail address: ibrahim.agwa@suezuniv.edu.eg (I.S. Agwa).

https://doi.org/10.1016/j.cscm.2023.e02266
Received 15 April 2023; Received in revised form 13 June 2023; Accepted 1 July 2023
Available online 1 July 2023

resources, such as limestone [2–4]. Crops produce a significant quantity of agricultural waste (AW) across the world, including rice husk ash [5], sugarcane ash [6], peanut husk ash[7], olive waste ashes[8], rice straw ash [9], sesame stalk ash [10] and palm oil fuel ash [11,12]. Recent studies have shown that ashes from diverse agricultural residues can be successfully used in the creation of concrete to lessen the use of cement and the disposal of AW[13].

Furthermore, multiple investigations have been recently undertaken to determine the effect of supplemental cementitious materials derived from industrial wastes (IW) on concrete features [14,15], such as ceramic waste [16],steel slag[17],ferrosilicon [18,19], fly ash [20], silica fume [21,22], phosphorous slag powder [23], and dehydrated cementitious powder produced by the heating treatment process of recycled construction waste cementitious materials [24]. Wang et al. [25] presented a practical method for producing UHPC by replacing fine natural river sand and cement with recycled gold tailings as IW. The findings showed that UHPC could have a comparatively high compressive strength over time and minimal leaching toxicity when full-scale recycling is applied.

Hence, mitigating environmental pollutants, such as water, soil, and air contamination, can be accomplished by inserting industrial and agricultural leftovers to replace part of the cement content in concrete manufacturing [26].

A significant quantity of AW is obtained through sugar production, including sugarcane leaf residues. These residues are burned to provide thermal energy to obtain sugarcane leaf ash (SLA) [27]. Sugarcane bagasse ash (SBA) is considered a pozzolanic substance; hence, numerous prior studies investigated its effect on concrete's qualities. Accordingly, SBA can be employed as a partial substitute for cement. Sugarcane bagasse is obtained from the residues of the sugar industry [28,29], and it differs from sugarcane leaves, which are represented in the leftovers from the sugarcane harvest [30]. This research aims to evaluate the effectiveness of utilizing SLA as a substitute for part of the cement content in manufacturing ultra-high-performance concrete (UHPC), building on the findings of earlier investigations on the use of SBA in the concrete industry [31,32]. A high concentration of binder during the manufacturing of UHPC results in the formation of an adequate and thick gel layer [33,34]. Given the significant quantity of cement needed to produce UHPC, replacing some cement with AW ash provides economic and environmental benefits and enhances UHPC's qualities [35,36]. Superior compressive strengths of 156 and 190 MPa were attained by replacing 17% and 20% of cement content with palm oil fuel ash and rice straw ash as fine AW ashes, respectively [37]. Amin et al. [38] studied the consequence of employing a new hybrid between palm leaf ash and nano cotton stalk ash in the concrete blend by replacing a quarter of the amount of cement with this hybrid. The results demonstrated an increase in the compressive strength (f_c) by approximately 16.94% over its original condition.

Meanwhile, the increasing demand for granite stone in construction caused a rise in the waste created throughout the stone-cutting and processing. Raw granite is processed via cutting, mashing, and buffing to obtain granite products for sale. Granite dust (GD) is one of the by-products created during this process and discarded. Meanwhile, the dried waste dust may become airborne particles [39], resulting in severe air pollution and causing other numerous environmental risks [40]. A number of studies have used GD as a replacement for fine aggregate within traditional concrete. Nevertheless, studies on the benefit of using GD as a partial substitute for cement content in UHPC are scarce.

Furthermore, recycling demolition debris as an alternative to aggregates maintains scarce natural resources while lessening waste's harmful environmental implications [41]. Some researchers have examined the characteristics of recycled fine aggregates (RFA). According to Solyman [42], the particles of RFA are more porous and irregular than those of natural fine aggregate (NFA). Evangelista and de Brito [43] concluded that employing RFA in producing structural concrete elements is suitable, with a replacement proportion of up to 30%. The greater the percentage of replacing NFA with RFA, the lower value of the f_c [44].

This research presents a novel study that compares SLA as AW with GD as IW in the UHPC creation without and with RFA. The influence of employing SLA or GD as partial replacements for cement on the characteristics of UHPC with replacement ratios of 20%, 30%, 40%, and 50% were investigated. Then, the optimum replacement ratio of SLA or GD from cement was adopted with further partial replacement of RFA from NFA with ratios ranging from 25% to 100% to evaluate the influence of RFA on the UHPC characteristics. The mixes were subjected to four diverse raised temperatures (200 °C, 400 °C, 600 °C, and 800 °C) to find the optimal heat treatment that would result in the finest UHPC characteristics. Several experiments, including slump flow, f_c, splitting tensile strength (f_{sp}), water permeability test, sorptivity coefficient test, and chloride permeability test, were performed to determine the effect of SLA and GD in addition to RFA on the UHPC attributes.This research also includes the findings of a microstructural examination of the various UHPC blends.

Table 1
Physical properties of binder materials.

Physical properties	Cement	SF	SLA	GD
Specific gravity	3.16	2.14	2.27	2.63
Initial setting time (min)	72	-	-	-
Final setting time (min)	307	-	-	-
Specific area (cm^2/gm)	3470	19890	12200	11400
Colour	Grey	Light Grey	Light Grey	Light Yellow

2. Experimental work

2.1. Materials

2.1.1. Cement and silica fume

Portland cement (CEM I 52.5 N) was employed in the current work, and its tests were conducted based on ASTM C150 [45]. While silica fume (SF) used in this work is a byproduct of the manufacturing of ferrosilicon alloys, Tables 1 and 2 list the characteristics of Portland cement and SF.

2.1.2. Sugarcane leaf ash and granite dust

As shown in Fig. 1, the leaves from sugarcane were gathered in the El-Mansoura region of Egypt for this investigation. The sugarcane leaf powder was calcined in an oven at 700 °C for 2 h at a heating rate of 10 °C/min [6]. After heating, the ashes can cool for one hour at room temperature. After that, the ashes were sieved, and particles passed through a sieve of size 75 μm. As revealed by eye inspection and SEM investigation, the physical properties of SLA are micro and nanoporous, and irregular, as shown in Fig. 2.

SLA chemical composition is detected through energy-dispersive X-ray (EDX) spectroscopy, as stated in Table 2. Granite was utilized in this study as industrial waste and collected from local fields in an industrial and construction zone in New Mansoura, Egypt. The pozzolanic effect of granite dust is used to partially substitute cement [46]. The physical and chemical properties of the granite dust are tabulated in Tables 1 and 2, respectively.

2.1.3. Quartz powder and fine aggregates

This study used quartz powder (QP) as a filler material with particle sizes between 10 and 50 μm. The physical properties and chemical compositions of QP are given in Tables 3 and 4, respectively. The current work used NFA and RFA in the experimental program to produce UHPC. The RFA utilized in the experiment was collected from the failure and crushing of concrete testing specimens in the materials and concrete laboratory of the Suez University of Technology and Education [47]. Testing on fine aggregates was done according to ASTM C33/C33M-18 [48]. The properties of the fine aggregates are summarised in Table 5. Fig. 3 depicts the grading curve of the fine aggregates utilized in the current work.

2.1.4. Steel fiber

The reinforcement ratio for UHPC is studied using steel fiber at varying powder concentrations. An adequate steel fiber dose for UHPC has been established at 1% volume [49]. According to the manufacturer, the properties of steel fibers are outlined in Table 6.

2.1.5. High rang water- reducing admixtures

High-range water-reducing (HRWR) superplasticizers (Viscocrete-3425) were used to achieve workability. It satisfies the ASTM-C-494 Type G standards for a superplasticizer [50] with a clear liquid color and a specific gravity of 1.09.

2.2. Mixtures proportion

To achieve the aims of this study, this investigation was conducted on three major groups, including a total of seventeen UHPC mixtures. Table 7 indicates the mix proportions for UHPC. The Portland cement (CEM I 52.5 N) was 1000 kg/m^3. SLA or GD is utilized to substitute Portland cement at 20%, 30%, 40%, and 50% by weight of cement. RFA is added as a partial replacement for fine aggregate in percentages of 25%, 50%, 75%, and 100% by volume. Steel fibers constitute about 1% of the volume of UHPC, while the water-to-binder ratio is 0.19. According to binder materials, the HRWR dose is 2.5%. (cement and SLA or GD). Using the previous research, four series of UHPC mixes with two types of pozzolanic materials (SLA and GD) and two types of fine aggregates (NFA and RFA) were created [51–53].

2.3. Sample preparation

The mixer was filled with fine aggregates and binder ingredients, and the blend became homogenous after nearly four minutes of

Table 2
Chemical compositions of binder materials.

Chemical compositions (%)	Cement	SF	SLA	GD
SiO_2	20.57	99.02	83.3	70.60
Al_2O_3	4.43	0.13	-	14.95
Fe_2O_3	2.98	0.19	-	2.02
CaO	62.54	0.12	10.46	2.63
MgO	3.28	0.13	0.76	0.85
SO_3	3.47	0.16	-	0.12
K_2O	0.94	0.10	7.37	4.94
Na_2O	0.82	0.05	0.90	3.89
LOI	0.97	0.10	-	-

Fig. 1. Strategy for producing sugarcane leaf ash: a) Cane green tops, b) Cane dry leaves, c) Sugarcane leaf was heated to 700 °C for 2 h, d) Sugarcane leaf ash.

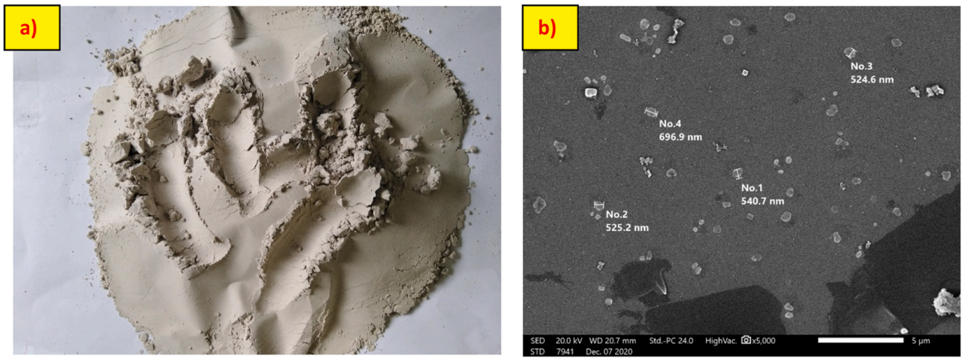

Fig. 2. a) Sugarcane leaf ash, b) SEM micrographs sugarcane leaf ash.

Table 3
Physical properties of the quartz powder.

Physical properties	Quartz Powder
Specific gravity	2.56
Specific area (cm^2/gm)	4450
Color	White

Table 4
Chemical compositions of the quartz powder.

Chemical compositions (%)	Quartz Powder
SiO_2	97.04
Al_2O_3	0.21
Fe_2O_3	0.28
CaO	0.60
SO_3	1.87

Table 5
The aggregates' mechanical and physical characteristics.

Properties	NFA	RFA
Specific gravity	2.67	2.65
Unit weight (kg/m^3)	1775	1720
Fineness modulus	2.43	2.62
Water absorption (%)	1.57	3.28
Clay and fine materials (%)	0.76	0.93

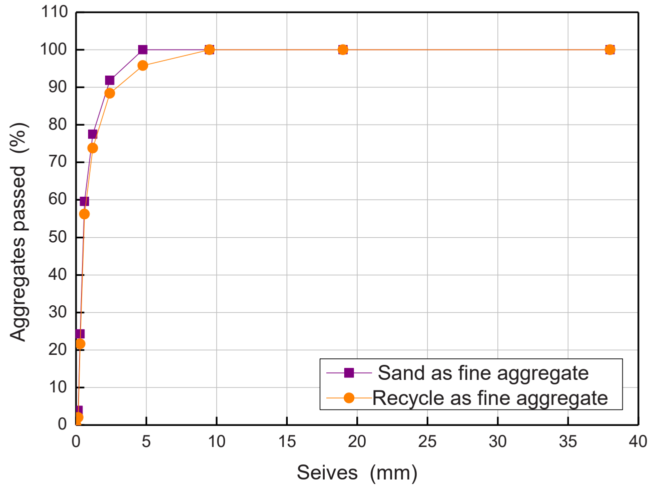

Fig. 3. Grading curve of aggregates.

Table 6
Steel fibers characteristics.

Length (mm)	Diameter (mm)	Aspect ratio	Tensile strength (MPa)	Modulus of elasticity (GPa)	Density (g/cm^3)
34	0.5	68	1980	190	7.80

Table 7
UHPC mixes' proportions, expressed in kg/m^3.

Mixture ID	Cement	SF	Quartz Powder	SLA	GD	NFA	RFA	Steel Fiber	HRWR	Water
CEM100-S100	1000	150	100	0	0	853.10	0	78	28.75	218.5
SLA20-S100	800	150	100	200	0	786.90	0	78	28.75	218.5
SLA30-S100	700	150	100	300	0	753.80	0	78	28.75	218.5
SLA40-S100	600	150	100	400	0	720.60	0	78	28.75	218.5
SLA50-S100	500	150	100	500	0	687.50	0	78	28.75	218.5
SLA20-S75R25	800	150	100	200	0	590.17	196.73	78	28.75	218.5
SLA20-S50R50	800	150	100	200	0	393.45	393.45	78	28.75	218.5
SLA20-S25R75	800	150	100	200	0	196.73	590.17	78	28.75	218.5
SLA20-R100	800	150	100	200	0	0	786.90	78	28.75	218.5
GD20-S100	800	150	100	0	200	819.0	0	78	28.75	218.5
GD30-S100	700	150	100	0	300	802.0	0	78	28.75	218.5
GD40-S100	600	150	100	0	400	785.0	0	78	28.75	218.5
GD50-S100	500	150	100	0	500	768.0	0	78	28.75	218.5
GD20-S75R25	800	150	100	0	200	614.25	204.75	78	28.75	218.5
GD20-S50R50	800	150	100	0	200	409.50	409.50	78	28.75	218.5
GD20-S25R75	800	150	100	0	200	204.75	614.25	78	28.75	218.5
GD20-R100	800	150	100	0	200	0	819.0	78	28.75	218.5

stirring. UHPC mixtures were poured and covered for twenty-four hours in the casting room. After twenty-four hours of casting, the specimens were extracted from the mould and put in the curing tank for water curing in accordance with ASTM C192 [54].

2.4. Test procedure

2.4.1. Fresh and hardened characteristics

In the current study, the fresh and hardened characteristics of UHPC were achieved. According to ASTM C1437[55], the slump flow was adopted to evaluate the workability of the fresh concrete condition. BS EN 12390–3[56] was used to measure the f_c utilizing universal testing equipment. Each mixture included three 100 mm × 100 mm × 100 mm cube specimens tested for f_c after one, seven, twenty-eight, and ninety days. The f_{sp} of UHPC was determined based on the ASTM C 496 technique [57]. At twenty-eight days, three cylindrical specimens with dimensions of 150 mm (diameter) and 300 mm (length) were adopted for each mixture. As stated by BS EN 12390–8 [58], the water permeability test was performed on cylindrical specimens of 150 mm (diameter) and 150 mm (length) after twenty-eight days. Chloride penetration resistance was determined using disc specimens with a diameter of 100 mm and thickness of

50 mm based on ASTM C1202 [59]. After twenty-eight days of casting, the approach specified in ASTM C1585–13 [60] was used to determine the water absorption rate. The present study looks at the f_c of concrete subjected to elevated temperatures. In accordance with BS EN 12390–3 [56], the 100 mm × 100 mm × 100 mm cube specimens were employed in this test. In the furnace. The heating strategy used here was similar to that employed by [16,38,61]. The specimens examined at temperatures 22 °C, 200 °C, 400 °C, 600 °C, and 800 °C for 2 h. Finally, the microstructure of the UHPC samples was analyzed via a scanning electronic microscope (SEM). The experimental program is implemented at the lab of the civil engineering department at El-Arish High Institute for Engineering and Technology, El-Arish, North Sinai, Egypt.

2.4.2. Hydration process of UHPC

In the presence of water, the silica in SLA and GD interacts with the Ca(OH)2 freed during cement hydration (pozzolanic reaction). This reaction produces extra calcium silicate hydrate (C-S-H) gel, which provides further homogenous tightly packed microstructures that improve the concrete characteristics.

3. Results and discussion

3.1. Fresh properties

3.1.1. Slump flow of UHPC

Fig. 4 displays the diameter value of the slump flow for every mix used in this study showing the effect of utilizing SLA and GD as partial substitutes for cement in UHPC on the slump value. This figure also depicts the consequence of employing RFA as a partial replacement for NFA on the slump flow of UHPC containing SLA or GD. The slump measurements in all mixes varied from 446 mm in the SLA50-S100 mix to 512 mm in the CEM100-S100 mix (Fig. 4). Incorporating SLA and GD into the concrete blend diminished the value of slump flow, which alludes to diminished workability, especially with the rise in the replacement ratio. For illustration, the diameter values of the slump flow dropped by approximately 2.93%, 6.25%, 9.77%, and 12.89% when the cement replacement ratios with SLA were 20%, 30%, 40%, and 50%, respectively, compared with the slump flow diameter of the control mix (CEM100-S100). Moreover, replacing the cement with GD by 20%, 30%, 40%, and 50% minimized the diameter values of the slump flow by approximately 1.95%, 5.08%, 8.20%, and 10.74%, respectively, compared with its value in the control mix (CEM100-S100). This result may be related to the binder's large surface area, which resulted from substituting a proportion from the cement weight by SLA or GD within the UHPC mix, which raised the need for water and lessened the free water quantity in the mixture [5,62]. Moreover, the ash particles of the sugarcane biomass are porous and have an irregular form [63,64].

Additionally, employing RFA as a partial substitute from NFA within the mix of UHPC, which contains a 20% SLA replacement ratio from cement weight, decreased the slump value compared with the control mix (CEM100-S100). These decreases were 3.32%, 4.30%, 6.64%, and 8.79% when the replacement ratios were 25%, 50%, 75%, and 100% (mixes SLA20-S75R25, SLA20-S50R50, SLA20-S25R75, and SLA20-R100), respectively. This slump value reduction results from the large internal friction force of RFA [65]. Moreover, the mixes that contain RFA and a 20% replacement ratio of GD from cement weight lessened the slump value compared with the control mix using the same replacement ratios of RFA (mixes GD20-S75R25, GD20-S50R50, GD20-S25R75, and GD20-R100).

Fig. 4 indicates that each mixture containing SLA has a lower slump flow than that of the corresponding mixture, which contains GD owing to the surface area of SLA being much higher than that of GD, as illustrated in Table 1.

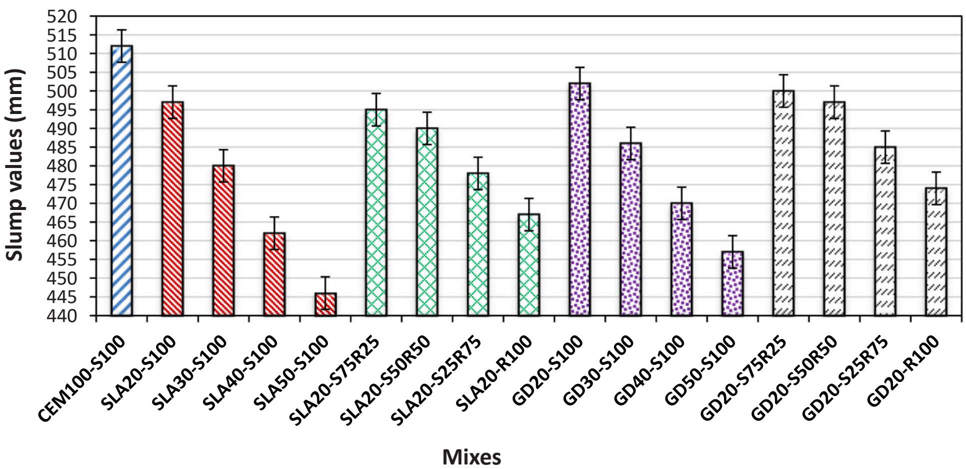

Fig. 4. Slump flow values of all tested UHPC mixes.

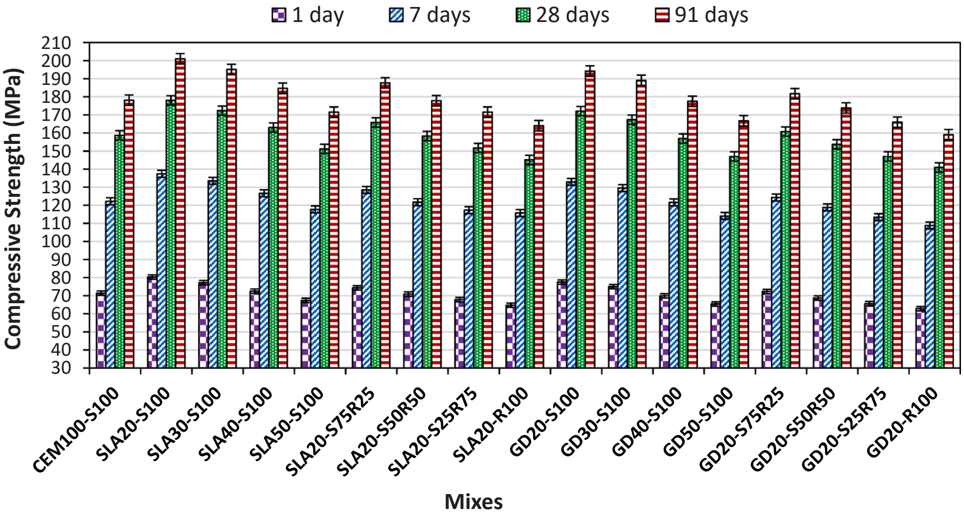

Fig. 5. Compressive strength findings of UHPC mixes at all test ages.

3.2. Mechanical properties

3.2.1. Compressive strength (f_c)

Fig. 5 demonstrates that the findings of the f_c test performed on the UHPC mixes after the curing at 1, 7, 28, and 29 days of casting showed that utilizing SLA as a partial alternative for cement up to 40% substitution ratio enhanced the f_c when compared with the control mix (CEM100-S100). Besides the effect of the large surface area accompanying SLA in stimulating the substance's pozzolanic reaction [66–68], the large concentration of SiO_2 at the amorphous stage reacts with $Ca(OH)_2$ and generates a further gel (C–S–H), which may contribute to the growth in the f_c value of the UHPC. However, using a 50% substitution ratio of SLA from cement slightly reduced the f_c compared with that of the control mix (CEM100-S100). The influence of high mitigation of cement amount may be the basis for this observation of the reduction in f_c value.

The control mixture presented 178.1 MPa f_c after 91 days of casting. However, the registered compressive strengths at the same test age were 201, 195.1, 184.7, and 171.5 MPa when SLA was incorporated into the UHPC mixture as a partial alternative from cement by 20%, 30%, 40%, and 50% (SLA20-S100, SLA30-S100, SLA40-S100, and SLA50-S100), respectively, as shown in Fig. 5. According to these results, the maximum f_c of UHPC was achieved at all test ages when SLA was incorporated into the mix as a partial alternative for cement by 20%.

After 28 days of casting, the f_c of UHPC mixes SLA20-S100, SLA30-S100, SLA40-S100, and SLA50-S100 within the second group recorded 178.0, 172.3, 163.0, and 151.2 MPa, respectively, showing an increase in the f_c by approximately 12.16%, 8.57%, and 2.71% at substitution ratios of 20%, 30%, and 40%, respectively, and a decrease in the f_c by nearly 4.73% at a substitution ratio of 50% compared with the control mix.

Fig. 5 shows that replacing the cement with GD in UHPC mixes up to 30% enhanced the f_c compared with the reference mix (CEM100-S100) after the same ages of casting mentioned above. This improvement in the f_c can be attributed to the effect of pore filling of extremely fine GD, which improves the hard density qualities of the interfacial transition zone product [69]. However, using 40% and 50% substitution ratios of GD from cement lessened f_c compared with the control mix (CEM100-S100). As previously mentioned [70,71], this phenomenon indicates that the f_c value of the UHPC mixes containing an exaggerated amount of GD is diminished due to the decrease of cement amount serving as the binder for the cement mortar. These findings agree well with earlier studies [71,72].

The registered compressive strengths after 28 days of the casting of mixes GD20-S100, GD30-S100, GD40-S100, and GD50-S100 within the third group were 172.1, 167.3, 156.9, and 147 MPa, showing a raised f_c of 8.44% and 5.42% at substitution ratios of 20% and 30% and a lowering in the f_c by 1.13% and 7.37% at substitution ratios of 40% and 50%, respectively, compared with the control mixture. These results demonstrated that the best substitution ratio of GD from the cement weight was 20%, which attained the maximum f_c of UHPC in the third group.

Meanwhile, using RFA as a partial substitute from NFA by 25% within the mix of UHPC with a 20% SLA substitution ratio from cement as in the mix SLA20-S75R25 has a positive influence on the f_c at all test ages (Fig. 5). Meanwhile, the f_c increased to 165.8 MPa with a 4.47% improvement over the control mix (CEM100-S100) after 28 days of casting. By contrast, increasing the substitution ratios of RFA to 50%, 75%, and 100% resulted in a reduction in f_c after 28 days of casting by 0.25%, 4.41%, and 8.57% (mixes SLA20-S50R50, SLA20-S25R75, and SLA20-R100), respectively. This phenomenon is attributed to the cement mortar included in RFA that reduces its crushing index to less than that of NFA, resulting in a weaker RFA strength than NFA. Another contributing factor is the poor interfacial transition zone between mortar and RFA compared with that between mortar and NFA [65].

Meanwhile, utilizing RFA as a partial substitute from NFA by 25% within the mix of UHPC with a 20% GD substitution ratio from cement as in the mix GD20-S75R25 improved the f_c at all test ages (Fig. 5). The f_c increased to 160.8 MPa with an improvement of 1.32% compared with the control mix (CEM100-S100) after 28 days of casting. However, increasing the substitution ratio of the RFA to 50%, 75%, and 100% caused a reduction in f_c by 3.15%, 7.37%, and 11.22% (mixes GD20-S50R50, GD20-S25R75, and GD20-R100), respectively.

The f_c of all UHPC mixes that contain RFA as a partial substitute from NFA and a 20% substitution ratio of SLA or GD from the cement weight is lower than that of UHPC mixes that contain a 20% substitution ratio of SLA or GD from the cement and without RFA (mixes SLA20-S100, and GD20-S100). This situation confirms the negative influence of using a high substitution ratio of RFA from NFA on the f_c of UHPC due to the weak strength of RFA. These findings are consistent with earlier investigations [73–75]. Finally, Fig. 5 shows that incorporating SLA into any mix in this work as a partial alternative for cement has a higher positive influence on the f_c value of UHPC than that of the corresponding mix, which contains GD because of the effect of SLA's large surface area on stimulating the substance's pozzolanic reaction [66–68].

3.2.2. Splitting tensile strength (f_{sp})

The outcomes of the f_{sp} test conducted on the UHPC mixes after 28 days of the curing demonstrated that utilizing SLA as a partial cement alternative up to a 30% substitution ratio boosted the f_{sp} compared with that of the control mix (CEM100-S100), as indicated in Fig. 6. Accordingly, the f_{sp} of UHPC mixes was found to be 9.44% and 5.93% larger than that of the control mix when the substitution ratios of the SLA from the cement weight were 20% and 30% (mixes SLA20-S100 and SLA30-S100), respectively. The f_{sp} was lower when the SLA was incorporated into the UHPC mix as a partial alternative for cement by 40% and 50% compared with the reference mix (CEM100-S100) (Fig. 6). This lowering was minimal (equivalent to 0.93%) in the case of a 40% substitution ratio, while it was significant (equivalent to 8%) in the case of a 50% substitution ratio (mixes SLA40-S100 and SLA50-S100, respectively). According to these outcomes, employing SLA as a partial alternative for cement by 20% showed the maximum f_{sp} for UHPC. These outcomes agree well with Agwa et al. [76].

Fig. 6 also presents the influence of replacing the cement with GD by up to 50% on the f_{sp} of UHPC after 28 days of curing. Utilizing GD as a partial alternative for cement up to a 30% substitution ratio improved the f_{sp} compared with the control mix (CEM100-S100). However, increasing the substitution ratio of GD from cement above this limit decreased the TS value compared with the control mix. The recorded f_{sp} values of mixes GD20-S100, GD30-S100, GD40-S100, and GD50-S100 were 17.96, 17.47, 16.19, and 15.17 MPa, showing an augmentation in the f_{sp} value by approximately 7%, and 4.07% at substitution ratios of 20% and 30% and decrease in the f_{sp} value by nearly 3.57% and 9.65% at substitution ratios of 40% and 50%, respectively, compared with those of the control mix. These results illustrated that the preferable substitution ratio of GD from the cement weight was 20%, which attained the utmost f_{sp} for UHPC in the third group. Accordingly, exaggerating the rate of replacing the cement with GD caused a negative influence on the f_{sp} of concrete. This finding was in agreement with previous studies [70,77].

Moreover, adding RFA to the mix of UHPC as a partial substitute from NFA by 25% in addition to using a 20% SLA substitution ratio from cement as in the mix SLA20-S75R25 boosted the f_{sp} of UHPC after 28 days of the curing (Fig. 6). The f_{sp} reached 17.32 MPa with an improvement of 3.15% compared with the control mix (CEM100-S100). By contrast, increasing the substitution ratio of RFA to 50%, 75%, and 100% caused a decrease in f_{sp} by approximately 0.36%, 3.5%, and 6.65% (mixes SLA20-S50R50, SLA20-S25R75, and SLA20-R100), respectively. In the same context, adding RFA to the mix of UHPC as a partial substitute from NFA by 25% in addition to using a 20% GD substitution ratio from cement as in the mix GD20-S75R25 upgraded the f_{sp} of the UHPC (Fig. 6). On the contrary, increasing the substitution ratio of RFA to 50%, 75%, and 100% (mixes GD20-S50R50, GD20-S25R75, and GD20-R100, respectively) caused a reduction in f_{sp} of the UHPC. Furthermore, the f_{sp} increased by approximately 2.29% higher than that of the control mix (CEM100-S100) at a substitution ratio of 25%, but it decreased by nearly 1.14%, 4.36%, and 7.36% compared with the control mixture

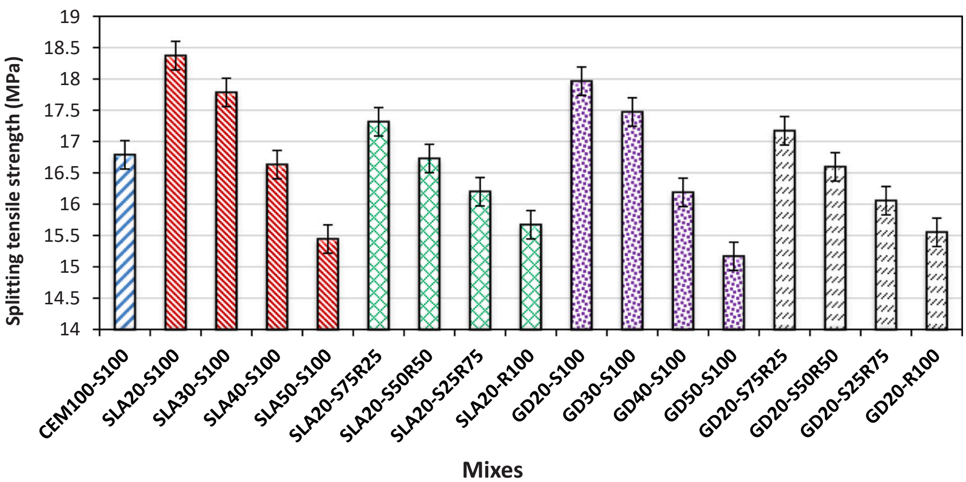

Fig. 6. Splitting tensile strength findings of UHPC mixes after twenty-eight days of the curing process.

at substitution ratios of 50%, 75%, and 100%, respectively. These findings about using RFA in concrete mixes are consistent with earlier studies [78–80].

The mixtures containing SLA presented a higher f_{sp} than those containing GD. All the outcomes in this section are due to the same factors discussed in the preceding section about f_c.

3.3. Transport properties of UHPC

3.3.1. Water permeability

Fig. 7 presents the findings of the water permeability test performed on all the UHPC mixes. This test demonstrated that adding SLA or GD to the blend as a partial cement alternative in the absence of RFA enhanced the efficacy of the UHPC by decreasing the mix water permeability for all substitution ratios applied in this test (20%, 30%, 40%, and 50%) compared with the reference mix (CEM100-S100). The microparticles of the cementitious material were used to seal the voids in the UHPC [81]. The SLA or GD helps the UHPC in lessening the pore volume in all UHPC mixes due to their pozzolanic activity, thus lessening water permeability [76,82,83].

The control mix (CEM100-S100) has 1.54×10^{-11} cm/s water permeability after 28 days of casting. Nevertheless, the UHPC water permeabilities of mixes SLA20-S100, SLA30-S100, SLA40-S100, and SLA50-S100 were 1.49×10^{-11} cm/s, 1.46×10^{-11} cm/s, 1.43×10^{-11} cm/s, and 1.38×10^{-11} cm/s, respectively, showing a decrease in the water permeability by approximately 3.25%, 5.19%, 7.14%, and 10.39% at substitution ratios of 20%, 30%, 40%, and 50%, respectively, compared with that of the reference mix. Mixes GD20-S100, GD30-S100, GD40-S100, and GD50-S100 have water permeability values of 1.51×10^{-11} cm/s, 1.48×10^{-11} cm/s, 1.45×10^{-11} cm/s, and 1.41×10^{-11} cm/s, showing a decrease in the water permeability by approximately 1.95%, 3.89%, 5.84%, and 8.44% at substitution ratios of 20%, 30%, 40%, and 50%, respectively, compared with that of the control mix. The water permeability value of the UHPC was the lowest for the mixes, in which 50% of cement was replaced by SLA or GD (Fig. 7). These results demonstrated that higher amounts of SLA or GD played a remarkable role in significantly reducing the concrete porosity as a consequence of the increased cementitious material hydration. These findings are consistent with comparable efforts [84,85].

Furthermore, employing RFA as a partial substitute from NFA by 25% within the mix of UHPC, which contains a 20% SLA substitution ratio from cement weight, positively affected the water permeability of the UHPC. The water permeability under this mixture decreased by 2.59% compared with that of the control mix (CEM100-S100) after 28 days of casting (mix SLA20-S75R25). However, increasing the substitution ratio of the RFA to 50%, 75%, and 100% resulted in an increase in the water permeability of the UHPC by 0.65%, 3.25%, and 5.84% (mixes SLA20-S50R50, SLA20-S25R75, and SLA20-R100, respectively). Moreover, mix GD20-S75R25, which contains a 25% substitution ratio of RFA from NFA and a 20% substitution ratio of GD from cement weight, lessened the water permeability of the UHPC by 1.29% compared with the control mix. By contrast, increasing the substitution ratios of the RFA to 50%, 75%, and 100% caused an increase in the water permeability of the UHPC by 1.95%, 5.19%, and 8.44% (mixes GD20-S50R50, GD20-S25R75, and GD20-R100), respectively. The water permeability of the UHPC increases when the substitution ratio of the RFA from NFA is excessively high, whether in mixes that contain SLA or GD (Fig. 7). This phenomenon can be ascribed to the comparatively porous remaining mortar stuck to the grains surface of recycled aggregate, which causes a decrease in concrete strength and a rise in water absorption in addition to the high water permeability [86]. These outcomes of the water permeability test in the presence of RFA within the concrete mix agree with the previous studies [86–89]. UHPC mixes containing GD displayed a higher water permeability than the UHPC mixes containing SLA, which may be ascribed to the lower surface area of GD compared with SLA, resulting in a lower pore-filling effect than SLA.

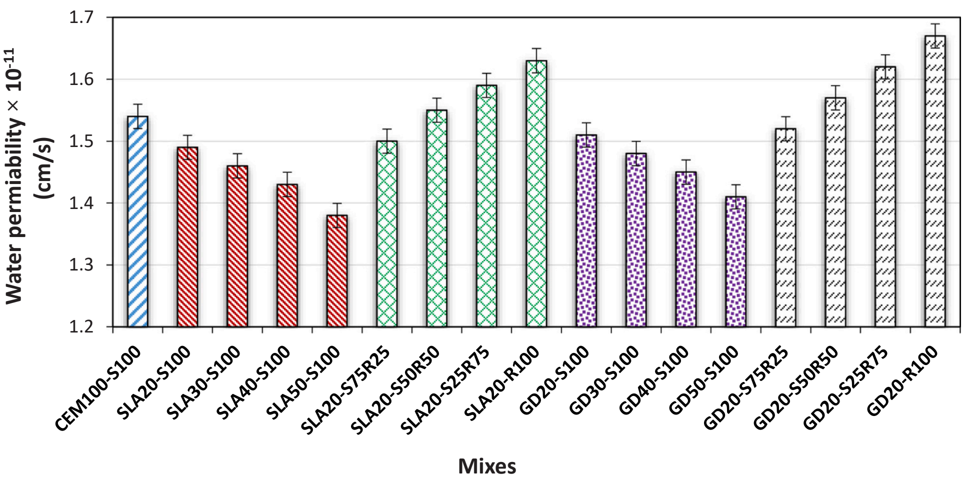

Fig. 7. Water permeability outcomes of UHPC mixes after twenty-eight days of the curing process.

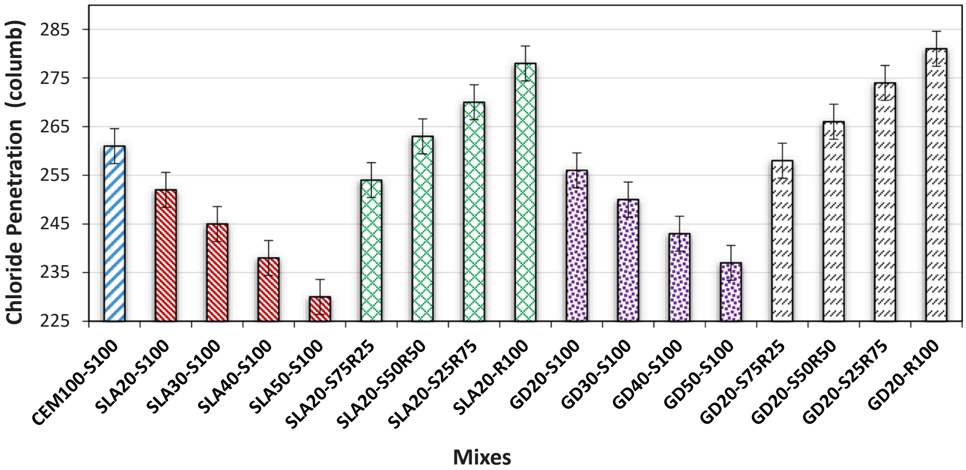

Fig. 8. Chloride penetration outcomes of UHPC mixes after twenty-eight days of the curing process.

3.3.2. Resistance to chloride penetration

Fig. 8 elucidates the effect of using SLA as AW and GD as IW on chloride penetration in the UHPC at the test age of 28 days. Employing SLA in UHPC mix as a partial cement alternative led to an improvement in the resistance of chloride penetration, and this enhancement continued with the increase in the substitution quantity. The chloride penetration test outcome of the control mix (CEM100-S100) was 261 C, and the chloride penetration values were reduced by 3.45%, 6.13%, 8.81%, and 11.88% with the employment of SLA at substitution ratios of 20%, 30%, 40%, and 50%, respectively. Furthermore, with the employment of GD, as a partial cement alternative at substitution ratios equal to 20%, 30%, 40%, and 50%, the chloride penetration was also improved, showing a reduction in its value by 1.92%, 4.4%, 6.89%, and 9.19%, respectively. This improvement may be attributed to the SLA and GD that were regularly distributed into the mixture and can seal the tiny voids, transitional zones, and fine cracks. This feature contributed to lessening the chloride penetration through the UHPC. Many investigations presented identical outcomes using other materials as partial alternatives for cement [9,90,91].

Moreover, adding RFA as a partial alternative from NFA by 25% in the mix of UHPC, which contains a 20% SLA substitution ratio from the cement weight, has a positive effect on the chloride penetration resistance, where the value of chloride penetration decreased by 2.68% compared with that of the control mix (CEM100-S100) after 28 days of casting. Meanwhile, increasing the substitution ratios of the RFA to 50%, 75%, and 100% resulted in an increase in the chloride penetration values through the UHPC by 0.77%, 3.45%, and 6.51%, respectively (Fig. 8). The UHPC mix, which contains a 25% substitution ratio of RFA from NFA and a 20% substitution ratio of GD from cement weight, reduced the chloride penetration value by 1.15% compared with the reference mix. However, increasing the substitution ratios of the RFA to 50%, 75%, and 100% caused an increase in the chloride penetration values through UHPC by 1.92%, 4.98%, and 7.66%, respectively (Fig. 8). The outcomes were in agreement with previous studies [80,92]. The detailed interpretations of the outcomes in this section are similar to those in the previous section about water permeability. The UHPC mixes with SLA presented a lower chloride permeability than those with GD. This outcome may be due to the difference in the surface area between the

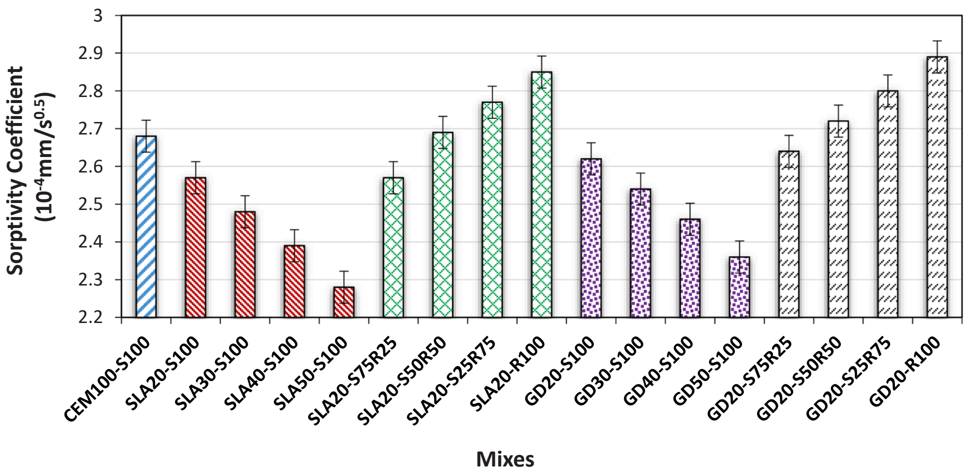

Fig. 9. Sorptivity coefficient outcomes of UHPC mixes after twenty-eight days of the curing process.

SLA and the GD, as explained in the preceding section.

3.3.3. Sorptivity coefficient

The sorptivity coefficient findings of all UHPC mixes containing AW represented in the SLA or IW represented in GD after 28 days of casting are displayed in Fig. 9. A compatible relationship between the water permeability test results and the sorptivity coefficient test outcomes was observed for each UHPC mix in this study. Incorporation of SLA or GD into the mix as a partial cement alternative in the absence of RFA boosted the efficiency of the UHPC by decreasing the mix sorptivity coefficient for all substitution ratios applied in this test (20%, 30%, 40%, and 50%) compared with the reference mix (CEM100-S100).

The control mix (CEM100-S100) has a sorptivity coefficient of 2.68 (10^{-4} mm/s$^{0.5}$) after 28 days of casting, while the UHPC sorptivity coefficients of mixes SLA20-S100, SLA30-S100, SLA40-S100, and SLA50-S100 decreased by 4.1%, 7.46%, 10.82%, and 14.93% at substitution ratios of 20%, 30%, 40%, and 50%, respectively, compared with that of the control mix (Fig. 9). Under the same approach, the sorptivity coefficients of mixes GD20-S100, GD30-S100, GD40-S100, and GD50-S100 decreased by 2.24%, 5.22%, 8.21%, and 11.94% at substitution ratios of 20%, 30%, 40%, and 50%, respectively, compared with that of the control mix (Fig. 9). These distinctive results can be attributed to the ability of SLA and GD to seal even the tiniest pores due to their tiny particle size and reduce the sorptivity rates.

Meanwhile, incorporating the RFA to the mixture of the UHPC as a partial substitute from NFA by 25%, in addition to a 20% SLA substitution ratio from the cement weight as in the mix SLA20-S75R25, reduced the sorptivity coefficient by 4.1% compared with that of the reference mix. However, increasing the substitution ratios of the RFA to 50%, 75%, and 100% caused a negative effect by increasing the sorptivity coefficients of the UHPC by 0.37%, 3.36%, and 6.34% (mixes SLA20-S50R50, SLA20-S25R75, and SLA20-R100), respectively (Fig. 9). Furthermore, mix GD20-S75R25, which contains a 25% substitution ratio of RFA from NFA and a 20% substitution ratio of GD from the cement weight, reduced the sorptivity coefficient of the UHPC by 1.49% compared with that of the reference mix. By contrast, increasing the substitution ratios of GD to 50%, 75%, and 100% increased the sorptivity coefficients of the UHPC by 1.49%, 4.48%, and 7.84% (mixes GD20-S50R50, GD20-S25R75, and GD20-R100), respectively (Fig. 9). Overall, the sorptivity coefficient was less in the UHPC mixes containing SLA than in the UHPC mixes containing GD.

3.4. Temperature studies

Fig. 10 shows the f_c results after 28 days of casting after heating UHPC mixes to 200 °C, 400 °C, 600 °C, and 800 °C for 2 h compared with the recorded f_c at the room temperature of 22 °C. This figure also illustrates the relationship between the different temperatures along the x-axis and the corresponding compressive strengths along the y-axis. Fig. 11 depicts the percentage of enhancement in the f_c for all heated mixes, which were subjected to 200 °C, and it may be attributed to the heating, which caused dry hardening and the continuous hydration of the cement particles that have already been hydrated [93–95]. These outcomes are consistent with prior studies [96,97]. The increment percentage of the f_c of the UHPC increased at 200 °C compared with that at room temperature by increasing the substitution ratio of SLA or GD as partial alternatives for cement weight (Fig. 11). The registered percentages for the improvement in the f_c for mixes CEM100-S100, SLA20-S100, SLA30-S100, SLA40-S100, and SLA50-S100 were 3.1%, 3.6%, 4%, 4.4%, and 4.7%, respectively. The improvement in f_c for mixes GD20-S100, GD30-S100, GD40-S100, and GD50-S100 under the same approach were 3.9%, 4.3%, 4.6%, and 4.9%, respectively. The percentage of improvement in the f_c also slightly increased when the ratio of using RFA as a partial substitute from NFA increased up to 75%, whether in mixes that contain SLA or GD at 200 °C; however, no change in the percentage of enhancement was observed in the f_c of the UHPC with an increase in the replacement ratio over that (Fig. 11).

When the mixes were exposed to higher temperatures (400 °C, 600 °C, and 800 °C), a noticeable decrease in the f_c value of the UHPC was observed for all heated mixes compared with its condition at room temperature (Fig. 11). This phenomenon may be attributed to the transformation of calcium hydroxide into calcium silicate hydrate at such exaggerated temperatures [98]. Furthermore, the f_c significantly decreased with rising temperature for each UHPC mix (Fig. 11). These findings are consistent with comparable efforts [34,99]. For example, mix CEM100-S100 showed compressive strengths of 127.4, 84.4, and 42.7 MPa at temperatures of 400 °C, 600 °C, and 800 °C, respectively. Furthermore, the percentage of decrease in the value of the f_c lessened as the substitution ratio of SLA or GD as partial alternatives for cement increased or as the RFA content as a partial substitute from NFA increased at a fixed substitution ratio of SLA or GD (Fig. 11). For example, mixes SLA20-S100, SLA30-S100, SLA40-S100, and SLA50-S100 demonstrated a percentage diminution in the f_c values by 43.2%, 41.5%, 39.6%, and 37.8% at a temperature of 600 °C, respectively. Finally, using GD in the UHPC buildings exposed to exaggerated temperatures is preferred over SLA. The percentage of decrease in the f_c value in the mixes containing SLA was higher than that in the mixes containing GD under the influence of high temperatures (Fig. 11).

3.5. Microstructure analysis

Figs. 12, 13, and 14 illustrate the SEM appearance of UHPC mixes CEM100-S100, SLA20-S100, and GD20-S100. The effects of utilizing 20% SLA or 20% GD as a partial cement replacement on the UHPC characteristics were investigated and compared with a control mixture by SEM at 28 days of casting using gradient imaging at high magnification from 2500 × to 10,000 × . The microstructure has enhanced due to the partial cement replacement with SLA or GD, as the SEM shows by lowering the pores inside the mixture. Fig. 13 demonstrates that the specimens of UHPC-SLA had the narrowest pore size and the maximum density. This finding agrees with the results of the mechanical and transport properties tests. Cement gel in the case of 10,000 × magnification is shown in Figs. 12b, 13b, and 14b, which were denser (less microporous size) when the SLA and GD were added compared with the control

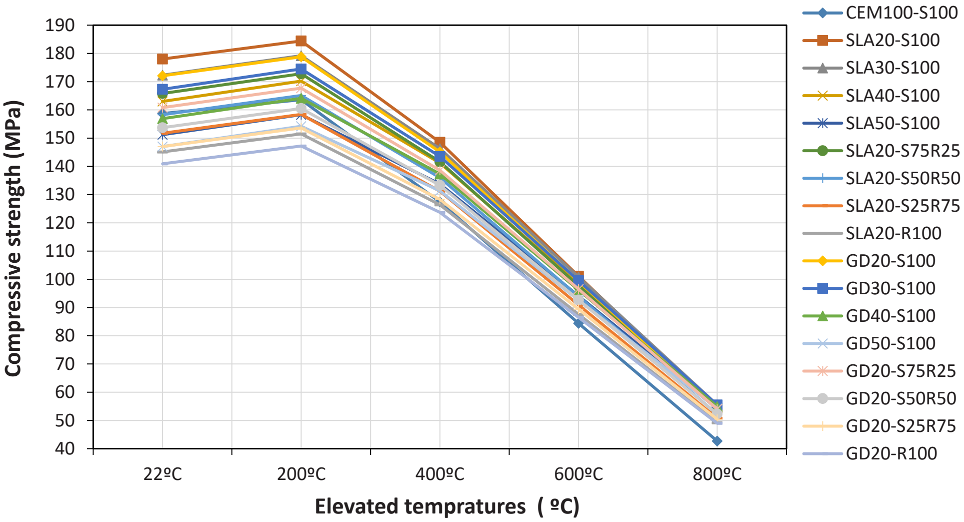

Fig. 10. The relation between different temperatures and the corresponding compressive strengths.

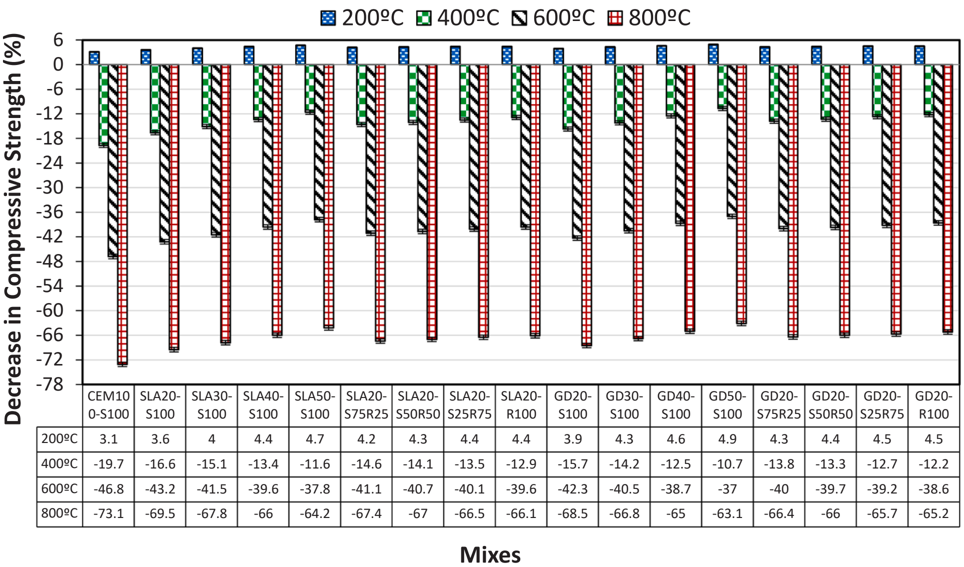

	CEM100-S100	SLA20-S100	SLA30-S100	SLA40-S100	SLA50-S100	SLA20-S75R25	SLA20-S50R50	SLA20-S25R75	SLA20-R100	GD20-S100	GD30-S100	GD40-S100	GD50-S100	GD20-S75R25	GD20-S50R50	GD20-S25R75	GD20-R100
200ºC	3.1	3.6	4	4.4	4.7	4.2	4.3	4.4	4.4	3.9	4.3	4.6	4.9	4.3	4.4	4.5	4.5
400ºC	-19.7	-16.6	-15.1	-13.4	-11.6	-14.6	-14.1	-13.5	-12.9	-15.7	-14.2	-12.5	-10.7	-13.8	-13.3	-12.7	-12.2
600ºC	-46.8	-43.2	-41.5	-39.6	-37.8	-41.1	-40.7	-40.1	-39.6	-42.3	-40.5	-38.7	-37	-40	-39.7	-39.2	-38.6
800ºC	-73.1	-69.5	-67.8	-66	-64.2	-67.4	-67	-66.5	-66.1	-68.5	-66.8	-65	-63.1	-66.4	-66	-65.7	-65.2

Fig. 11. The percentage of reduction in the value of compressive strength of UHPC mixes after twenty-eight days of the curing process under the influence of various high temperatures.

mixture (Fig. 12b). The large proportion of amorphous SiO_2 in the SLA and GD and the packing capability of the UHPC matrix may be attributed to the enhancement in the microstructure and properties of the UHPC. Several elements were exhibited, including 1) the great smoothness and spherical properties, which assisted in replacing the water caught between the fine and coarse particles. [100]; 2) the influence on the flow of the blend (reduces flow reluctance) as a well-dispersed multiphase system with an intensive microstructure and low permeability [101]. 3) The interaction with calcium hydroxide led to the creation of an extra gel, which caused the creation of a thick and strong C–S–H gel [102].

4. Conclusions

This research presented a novel study that involved a comparison of employing SLA (derived from AW) with GD (derived from IW) as partial replacements for cement in the production of eco-friendly UHPC and a discussion of the effect of these materials on the mechanical and transport properties of UHPC through the experimental investigations. Additionally, this research investigated the effect of using RFA as a partial replacement for NFA on the UHPC qualities in the presence of SLA or GD. The following main conclusions were drawn based on the experimental findings in this research:

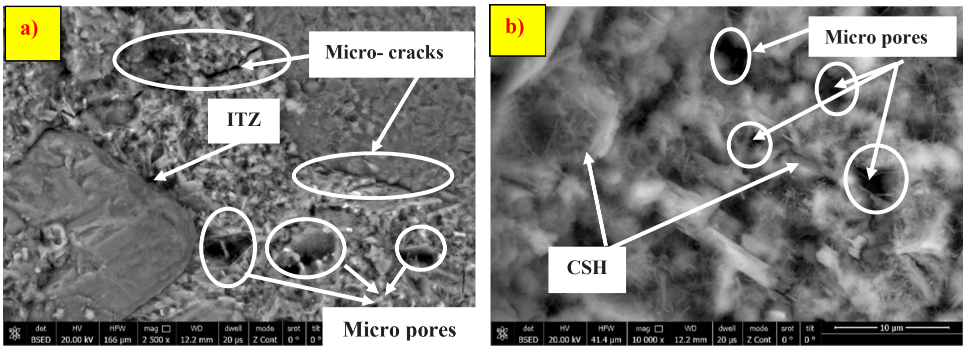

Fig. 12. SEM images of CEM100-S100, a) 2500 × magnification, b) 10000 × magnification.

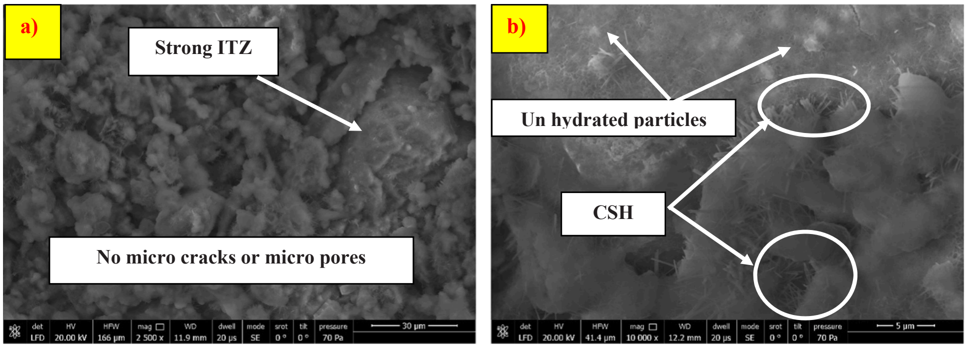

Fig. 13. SEM images of SLA20-S100, a) 2500 × magnification, b) 10000 × magnification.

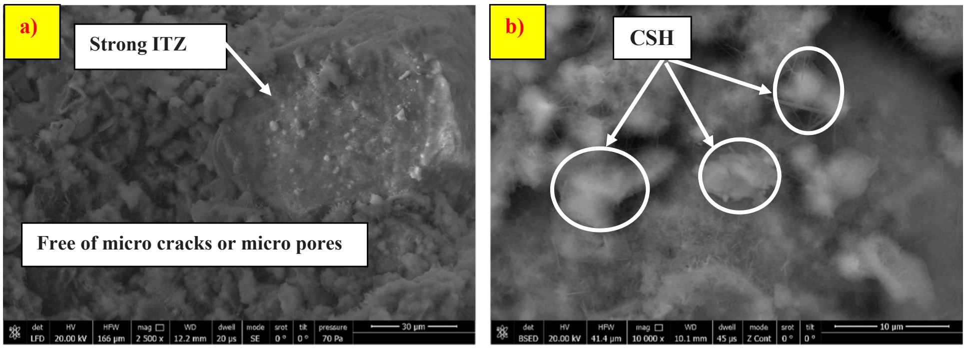

Fig. 14. SEM images of GD20-S100, a) 2500 × magnification, b) 10000 × magnification.

- Each mix containing SLA has a lower slump flow than the corresponding mix, which contains GD by a value ranging from 1% to 2.47% when the cement replacement ratios range from 20% to 50%.
- The best replacement ratio of SLA or GD from the cement weight was 20%, which gave the maximum f_c and f_{sp} compared with the other substitution proportions in both applied replacement cases.
- Using RFA as a partial replacement from NFA by 25% within the mix of UHPC with a 20% substitution ratio of SLA or GD from cement has a beneficial influence on the f_c and f_{sp}.
- Incorporating SLA into any mix as a partial substitute for cement achieved a higher positive effect on the values of f_c and f_{sp} of UHPC than those of a similar mix containing GD.
- The transport properties of the UHPC were significantly improved by adding SLA or GD to the mixture as a partial cement replacement, especially at a 50% substitution ratio.
- Increasing the substitution ratio of SLA or GD caused an increase in the increment percentage of f_c of the UHPC at 200 °C compared with that at room temperature.
- The percentage of improvement in the f_c slightly increased when the substitution ratio of the RFA increased up to 75% at 200 °C.

- The percentage of decrease in the f_c value at the exaggerated temperatures in the mixes containing SLA was higher than that in the mixes containing GD.

Declaration of Competing Interest

The authors declare that they have no known competing financial interests or personal relationships that could have appeared to influence the work reported in this paper.

Data Availability

No data was used for the research described in the article.

Acknowledgment

Authors would like to acknowledge the support of the Deputyship for Research and Innovation- Ministry of Education, Kingdom of Saudi Arabia for this research through a grant (NU/IFC/2/SERC/-/24) under the institutional Funding Committee at Najran University, Kingdom of Saudi Arabia.

References

[1] A. Singh, R. Kumar, P. Mehta, D. Tripathi, Effect of nitric acid on rice husk ash steel fiber reinforced concrete, Mater. Today.: Proc. 27 (2020) 995–1000.
[2] D.N. Huntzinger, T.D. Eatmon, A life-cycle assessment of Portland cement manufacturing: comparing the traditional process with alternative technologies, J. Clean. Prod. 17 (7) (2009) 668–675.
[3] Y. Lei, Q. Zhang, C. Nielsen, K. He, An inventory of primary air pollutants and CO_2 emissions from cement production in China, 1990–2020, Atmos. Environ. 45 (1) (2011) 147–154.
[4] V. Kanthe, Effect of superplasticizer on strength and durability of rice husk ash concrete, Iran. J. Energy Environ. 12 (3) (2021) 204–208.
[5] I.S. Agwa, O.M. Omar, B.A. Tayeh, B.A. Abdelsalam, Effects of using rice straw and cotton stalk ashes on the properties of lightweight self-compacting concrete, Constr. Build. Mater. 235 (2020), 117541.
[6] M. Amin, M.M. Attia, I.S. Agwa, Y. Elsakhawy, K. Abu El-hassan, B.A. Abdelsalam, Effects of sugarcane bagasse ash and nano eggshell powder on high-strength concrete properties, Case Stud. Constr. Mater. 17 (2022), e01528.
[7] M.H. Abd-Elrahman, I.S. Agwa, S.A. Mostafa, O. Youssf, Effect of utilizing peanut husk ash on the properties of ultra-high strength concrete, Constr. Build. Mater. 384 (2023), 131398.
[8] I.Y. Hakeem, I.S. Agwa, B.A. Tayeh, M.H. Abd-Elrahman, Effect of using a combination of rice husk and olive waste ashes on high-strength concrete properties, Case Stud. Constr. Mater. 17 (2022), e01486.
[9] M. Amin, B.A. Tayeh, M.A. Kandil, I.S. Agwa, M.F. Abdelmagied, Effect of rice straw ash and palm leaf ash on the properties of ultrahigh-performance concrete, Case Stud. Constr. Mater. 17 (2022), e01266.
[10] I.Y. Hakeem, M. Amin, A.M. Zeyad, B.A. Tayeh, A.M. Maglad, I.S. Agwa, Effects of nano sized sesame stalk and rice straw ashes on high-strength concrete properties, J. Clean. Prod. 370 (2022), 133542.
[11] A.M. Zeyad, M.A.M. Johari, B.A. Tayeh, M.O. Yusuf, Pozzolanic reactivity of ultrafine palm oil fuel ash waste on strength and durability performances of high strength concrete, J. Clean. Prod. 144 (2017) 511–522.
[12] A.M. Zeyad, M.A.M. Johari, A. Abutaleb, B.A. Tayeh, The effect of steam curing regimes on the chloride resistance and pore size of high–strength green concrete, Constr. Build. Mater. 280 (2021), 122409.
[13] A.R. de Azevedo, M. Amin, M. Hadzima-Nyarko, I.S. Agwa, A.M. Zeyad, B.A. Tayeh, A. Adesina, Possibilities for the application of agro-industrial wastes in cementitious materials: a brief review of the Brazilian perspective, Cleaner, Materials 3 (2022), 100040.
[14] W. Huang, H. Kazemi-Kamyab, W. Sun, K. Scrivener, Effect of replacement of silica fume with calcined clay on the hydration and microstructural development of eco-UHPFRC, Mater. Des. 121 (2017) 36–46.
[15] B.A. Tayeh, B.H. Abu Bakar, M. Johari, A.M. Zeyad, The role of silica fume in the adhesion of concrete restoration systems, Adv. Mater. Res. (2013) 265–269.
[16] M. Amin, A.M. Zeyad, B.A. Tayeh, I.S. Agwa, Engineering properties of self-cured normal and high strength concrete produced using polyethylene glycol and porous ceramic waste as coarse aggregate, Constr. Build. Mater. 299 (2021), 124243.
[17] M.M. Attia, B.A. Abdelsalam, M. Amin, I.S. Agwa, M.F. Abdelmagied, Metal-nails waste and steel slag aggregate as alternative and eco-friendly radiation shielding composites, Buildings 12 (8) (2022) 1120.
[18] A.M. Heniegal, M. Amin, S. Nagib, H. Youssef, I.S. Agwa, Effect of nano ferrosilicon and heavyweight fine aggregates on the properties and radiation shielding of ultra-high performance heavyweight concrete, Case Stud. Constr. Mater. 17 (2022), e01543.
[19] M.H. Abd-Elrahman, I.S. Agwa, Y. Elsakhawy, M.S. Rizk, Effect of utilising ferrosilicon and recycled steel fibres on ultra-high-strength concrete containing recycled granite, Case Stud. Constr. Mater. 18 (2023), e01903.
[20] A.A.J. Ghanim, M. Amin, A.M. Zeyad, B.A. Tayeh, I.S. Agwa, Effect of modified nano-titanium and fly ash on ultra-high-performance concrete properties, Struct. Concr. (2023).
[21] Z. Wu, K.H. Khayat, C. Shi, Changes in rheology and mechanical properties of ultra-high performance concrete with silica fume content, Cem. Concr. Res. 123 (2019), 105786.
[22] T.A. Tawfik, K.A. Metwally, S. El-Beshlawy, D.M. Al Saffar, B.A. Tayeh, H.S. Hassan, Exploitation of the nanowaste ceramic incorporated with nano silica to improve concrete properties, J. King Saud. Univ. -Eng. Sci. 33 (8) (2021) 581–588.
[23] Y. Huang, G. Chen, R. Yang, R. Yu, R. Xiao, Z. Wang, G. Xie, J. Cheng, Hydration kinetics and microstructure development of ultra-high performance concrete (UHPC) by high volume of phosphorus slag powder, Cem. Concr. Compos. 138 (2023), 104978.
[24] D. Qian, R. Yu, Z. Shui, Y. Sun, C. Jiang, F. Zhou, M. Ding, X. Tong, Y. He, A novel development of green ultra-high performance concrete (UHPC) based on appropriate application of recycled cementitious material, J. Clean. Prod. 261 (2020), 121231.
[25] J. Wang, R. Yu, W. Xu, C. Hu, Z. Shui, D. Qian, Y. Leng, K. Liu, D. Hou, X. Wang, A novel design of low carbon footprint ultra-high performance concrete (UHPC) based on full scale recycling of gold tailings, Constr. Build. Mater. 304 (2021), 124664.
[26] C.M. Grădinaru, A.A. Şerbănoiu, D.T. Babor, G.C. Sârbu, I.V. Petrescu-Mag, A.C. Grădinaru, When agricultural waste transforms into an environmentally friendly material: the case of green concrete as alternative to natural resources depletion, J. Agric. Environ. Ethics 32 (1) (2019) 77–93.
[27] Q. Xu, T. Ji, S.-J. Gao, Z. Yang, N. Wu, Characteristics and applications of sugar cane bagasse ash waste in cementitious materials, Materials 12 (1) (2018) 39.
[28] T. Klathae, T.N.H. Tran, S. Men, C. Jaturapitakkul, W. Tangchirapat, Strength, chloride resistance, and water permeability of high volume sugarcane bagasse ash high strength concrete incorporating limestone powder, Constr. Build. Mater. 311 (2021), 125326.

[29] N. Wu, T. Ji, P. Huang, T. Fu, X. Zheng, Q. Xu, Use of sugar cane bagasse ash in ultra-high performance concrete (UHPC) as cement replacement, Constr. Build. Mater. 317 (2022), 125881.
[30] J.B. Jamora, S.E.L. Gudia, A.W. Go, M.B. Giduquio, J.W.A. Orilla, M.E. Loretero, Potential reduction of greenhouse gas emission through the use of sugarcane ash in cement-based industries: a case in the Philippines, J. Clean. Prod. 239 (2019), 118072.
[31] M.J. Khalil, M. Aslam, S. Ahmad, Utilization of sugarcane bagasse ash as cement replacement for the production of sustainable concrete–a review, Constr. Build. Mater. 270 (2021), 121371.
[32] S. Deepika, G. Anand, A. Bahurudeen, M. Santhanam, Construction products with sugarcane bagasse ash binder, J. Mater. Civ. Eng. 29 (10) (2017), 04017189.
[33] O. Mishra, S. Singh, An overview of microstructural and material properties of ultra-high-performance concrete, J. Sustain. Cem. -Based Mater. 8 (2) (2019) 97–143.
[34] M. Amin, B.A. Tayeh, I.S. Agwa, Effect of using mineral admixtures and ceramic wastes as coarse aggregates on properties of ultrahigh-performance concrete, J. Clean. Prod. 273 (2020), 123073.
[35] S. Chandra Paul, P.B. Mbewe, S.Y. Kong, B. Šavija, Agricultural solid waste as source of supplementary cementitious materials in developing countries, Materials 12 (7) (2019) 1112.
[36] B.A. Tayeh, B.A. Bakar, M. Johari, Mechanical properties of old concrete-UHPFC interface, International Conference on Concrete Repair, Rehabilitation and Retrofitting, 2012, pp. 02–05.
[37] N. Van Tuan, G. Ye, K. Van Breugel, A.L. Fraaij, D. Dai Bui, The study of using rice husk ash to produce ultra high performance concrete, Constr. Build. Mater. 25 (4) (2011) 2030–2035.
[38] M. Amin, A.M. Zeyad, B.A. Tayeh, I.S. Agwa, Effects of nano cotton stalk and palm leaf ashes on ultrahigh-performance concrete properties incorporating recycled concrete aggregates, Constr. Build. Mater. 302 (2021), 124196.
[39] R. Lakhani, R. Kumar, P. Tomar, Utilization of stone waste in the development of value added products: a state of the art review, J. Eng. Sci. Technol. Rev. 7 (3) (2014).
[40] G. Rego, C. Martinez, A. Quero, T. Blanco, J. Borquea, The effects of dust inhalation in slate industry workers, Med. Clin. 116 (8) (2001) 290–291.
[41] J. De Brito, J. Ferreira, J. Pacheco, D. Soares, M. Guerreiro, Structural, material, mechanical and durability properties and behaviour of recycled aggregates concrete, J. Build. Eng. 6 (2016) 1–16.
[42] M. Solyman, Classification of recycled sands and their applications as fine aggregates for concrete and bituminous mixtures, 2005.
[43] L. Evangelista, J. De Brito, Mech. Behav. Concr. made fine Recycl. Concr. Aggreg., Cem. Concr. Compos. 29 5 2007 397 401.
[44] J.M. Khatib, Properties of concrete incorporating fine recycled aggregate, Cem. Concr. Res. 35 (4) (2005) 763–769.
[45] A.Sf Testing Mater., Stand. Specif. Portland Cem., ASTM C150 2018.
[46] A. Danish, M.A. Mosaberpanah, M.U. Salim, R. Fediuk, M.F. Rashid, R.M. Waqas, Reusing marble and granite dust as cement replacement in cementitious composites: a review on sustainability benefits and critical challenges, J. Build. Eng. 44 (2021), 102600.
[47] Y. Wang, P. Hughes, H. Niu, Y. Fan, A new method to improve the properties of recycled aggregate concrete: Composite addition of basalt fiber and nano-silica, J. Clean. Prod. 236 (2019), 117602.
[48] A. ASTM C33/C33M-18: Standard Specification for Concrete Aggregates, ASTM International West Conshohocken (PA) 2018 2018.
[49] R. Yu, P. Spiesz, H. Brouwers, Mix design and properties assessment of ultra-high performance fibre reinforced concrete (UHPFRC), Cem. Concr. Res. 56 (2014) 29–39.
[50] C. ASTM, 494/C494 M-99a,"Standard Specification for Chemical Admixtures for Concrete". PA, ASTM International, West Conshohocken, 2015.
[51] M. Amin, I.Y. Hakeem, A.M. Zeyad, B.A. Tayeh, A.M. Maglad, I.S. Agwa, Influence of recycled aggregates and carbon nanofibres on properties of ultra-high-performance concrete under elevated temperatures, Case Stud. Constr. Mater. 16 (2022), e01063.
[52] M. Amin, A.M. Zeyad, B.A. Tayeh, I.S. Agwa, Effect of ferrosilicon and silica fume on mechanical, durability, and microstructure characteristics of ultra high-performance concrete, Constr. Build. Mater. 320 (2022), 126233.
[53] I.Y. Hakeem, M. Amin, B.A. Abdelsalam, B.A. Tayeh, F. Althoey, I.S. Agwa, Effects of nano-silica and micro-steel fiber on the engineering properties of ultra-high performance concrete, Struct. Eng. Mech. 82 (3) (2022) 295–312.
[54] A. International, ASTM C192/C192M-19, standard practice for making and curing concrete test specimens in the laboratory, Am. Soc. Test. Mater. (2019).
[55] C. ASTM, Standard test method for flow of hydraulic cement mortar, C1437 (2007).
[56] BSI., BS EN 12390–3: 2019: Testing Hardened Concrete. Part 3: Compressive Strength of Test Specimens, BSI British Standards Institution2022.
[57] A. International, ASTM C496/C496M-17, Standard Test Method for Splitting Tensile Strength of Cylindrical Concrete Specimens, ASTM International, West Conshohocken, 2017.
[58] B.E. 12390-8 Testing Hardened Concrete Depth Penetration Water Press., Br. Stand. Inst. Lond., UK 2019.
[59] A. C, Standard Test Method for Electrical Indication of Concrete's Ability to Resist Chloride Penetration. Annual Book of ASTM Standards, American Society of Testing and Materials, West Conshohocken, 2009.
[60] A.S.T.M. ASTM, ."C1585-13." Standard Test Method for Measurement of Rate of Absorption of Water by Hydraulic-Cement Concretes, American Society for Testing and Materials West Conshohocken, PA, USA, 2013, p. 2013.
[61] R.T.C.-H.U.s.t.a. at, Recommendation of RILEM TC 200-HTC: mechanical concrete properties at high temperatures—modelling and applications: Part 1: Introduction—General presentation, Mater. Struct. 40 (2007) 841–853.
[62] I.S. Agwa, A.M. Zeyad, B.A. Tayeh, A. Adesina, A.R. de Azevedo, M. Amin, M. Hadzima-Nyarko, A comprehensive review on the use of sugarcane bagasse ash as a supplementary cementitious material to produce eco-friendly concretes, Mater. Today.: Proc. (2022).
[63] V.D. Katare, M.V. Madurwar, Experimental characterization of sugarcane biomass ash–A review, Constr. Build. Mater. 152 (2017) 1–15.
[64] M.A. C.d.A. Larissa, M.V. dos Anjos, N.S. de Sá, E.C. de Souza, de Farias, Effect of high temperatures on self-compacting concrete with high levels of sugarcane bagasse ash and metakaolin, Constr. Build. Mater. 248 (2020), 118715.
[65] D. Gao, F. Wang, Effects of recycled fine aggregate and steel fiber on compressive and splitting tensile properties of concrete, J. Build. Eng. 44 (2021), 102631.
[66] J. Martirena-Hernandez, S. Betancourt-Rodriguez, B. Middendorf, A. Rubio, J. Martinez-Fernandez, J.M. López, R. González-López, Pozzolanic properties of residues of sugar industries (first part), Mater. De. Constr. 50 (260) (2000) 71–78.
[67] J. Martirena-Hernández, S. Betancourt-Rodriguez, B. Middendorf, A. Rubio, L. Martínez-Fernández, I.M. López, R. González-López, Pozzolanic properties of residues of sugar industries (second part), Mater. De. Constr. 51 (261) (2001) 67–72.
[68] J. Payá, J. Monzó, M.V. Borrachero, L. Díaz-Pinzón, L.M. Ordonez, Sugar-cane bagasse ash (SCBA): studies on its properties for reusing in concrete production, J. Chem. Technol. Biotechnol.: Int. Res. Process Environ. Clean. Technol. 77 (3) (2002) 321–325.
[69] S. Ghorbani, I. Taji, J. De Brito, M. Negahban, S. Ghorbani, M. Tavakkolizadeh, A. Davoodi, Mechanical and durability behaviour of concrete with granite waste dust as partial cement replacement under adverse exposure conditions, Constr. Build. Mater. 194 (2019) 143–152.
[70] S. Abukersh, C. Fairfield, Recycled aggregate concrete produced with red granite dust as a partial cement replacement, Constr. Build. Mater. 25 (10) (2011) 4088–4094.
[71] A. Rana, P. Kalla, L.J. Csetenyi, Sustainable use of marble slurry in concrete, J. Clean. Prod. 94 (2015) 304–311.
[72] R. Hamza, S. El-Haggar, S. Khedr, Utilization of marble and granite waste in concrete bricks 2011 Int. Conf. Environ. Biosci. IPCBEE 2011.
[73] S. Kou, C.S. Poon, Properties of self-compacting concrete prepared with coarse and fine recycled concrete aggregates, Cem. Concr. Compos. 31 (9) (2009) 622–627.
[74] P. Pereira, L. Evangelista, J. De, Brito, The effect of superplasticisers on the workability and compressive strength of concrete made with fine recycled concrete aggregates, Constr. Build. Mater. 28 (1) (2012) 722–729.
[75] J.A. Bogas, J. De Brito, D. Ramos, Freeze–thaw resistance of concrete produced with fine recycled concrete aggregates, J. Clean. Prod. 115 (2016) 294–306.
[76] I.S. Agwa, A.M. Zeyad, B.A. Tayeh, M. Amin, Effect of different burning degrees of sugarcane leaf ash on the properties of ultrahigh-strength concrete, J. Build. Eng. (2022), 104773.

[77] L. Li, Y. Wang, Y. Tan, A. Kwan, L. Li, Adding granite dust as paste replacement to improve durability and dimensional stability of mortar, Powder Technol. 333 (2018) 269–276.
[78] R. Kumar, S.C.B. Gurram, A.K. Minocha, Influence of recycled fine aggregate on microstructure and hardened properties of concrete, Mag. Concr. Res. 69 (24) (2017) 1288–1295.
[79] P. Pereira, L. Evangelista, J. De Brito, The effect of superplasticizers on the mechanical performance of concrete made with fine recycled concrete aggregates, Cem. Concr. Compos. 34 (9) (2012) 1044–1052.
[80] A. Mardani-Aghabaglou, M. Tuyan, K. Ramyar, Mechanical and durability performance of concrete incorporating fine recycled concrete and glass aggregates, Mater. Struct. 48 (8) (2015) 2629–2640.
[81] P. Mehta Studies on the mechanisms by which condensed silica fume improves the properties of concrete: durability aspects Proc. Int. Workshop Condens. silica fume Concr., Ott. 1987 1 17.
[82] S. Praveenkumar, G. Sankarasubramanian, S. Sindhu, Selecting optimized mix proportion of bagasse ash blended high performance concrete using analytical hierarchy process (AHP), Comput. Concr. 23 (6) (2019) 459–470.
[83] M. Rashwan, T. Al-Basiony, A. Mashaly, M. Khalil, Behaviour of fresh and hardened concrete incorporating marble and granite sludge as cement replacement, J. Build. Eng. 32 (2020), 101697.
[84] E. Ghafari, H. Costa, E. Júlio, A. Portugal, L. Durães, The effect of nanosilica addition on flowability, strength and transport properties of ultra high performance concrete, Mater. Des. 59 (2014) 1–9.
[85] A. Tafraoui, G. Escadeillas, T. Vidal, Durability of the ultra high performances concrete containing metakaolin, Constr. Build. Mater. 112 (2016) 980–987.
[86] V.W. Tam, M. Soomro, A.C.J. Evangelista, A. Haddad, Deformation and permeability of recycled aggregate concrete-a comprehensive review, J. Build. Eng. 44 (2021), 103393.
[87] R. Singh, D. Nayak, A. Pandey, R. Kumar, V. Kumar, Effects of recycled fine aggregates on properties of concrete containing natural or recycled coarse aggregates: a comparative study, J. Build. Eng. 45 (2022), 103442.
[88] J. Dang, J. Xiao, Z. Duan, Effect of pore structure and morphological characteristics of recycled fine aggregates from clay bricks on mechanical properties of concrete, Constr. Build. Mater. 358 (2022), 129455.
[89] M. Nedeljković, J. Visser, B. Šavija, S. Valcke, E. Schlangen, Use of fine recycled concrete aggregates in concrete: a critical review, J. Build. Eng. 38 (2021), 102196.
[90] R. Gopalakrishnan, R. Jeyalakshmi, The effects on durability and mechanical properties of multiple nano and micro additive OPC mortar exposed to combined chloride and sulfate attack, Mater. Sci. Semicond. Process. 106 (2020), 104772.
[91] A. Pandey, B. Kumar, A comprehensive investigation on application of microsilica and rice straw ash in rigid pavement, Constr. Build. Mater. 252 (2020), 119053.
[92] L. Evangelista, J. de Brito, Durability of crushed fine recycled aggregate concrete assessed by permeability-related properties, Mag. Concr. Res. 71 (21) (2019) 1142–1150.
[93] D. Tobbala, B.A. Abdelsalam, I.S. Agwa, Bond performance of a hybrid coating zinc-rich epoxy incorporating nano-ferrite for steel rebars subjected to high temperatures in concrete, J. Build. Eng. 32 (2020), 101698.
[94] M. Amin, A.M. Zeyad, B.A. Tayeh, I.S. Agwa, Effect of high temperatures on mechanical, radiation attenuation and microstructure properties of heavyweight geopolymer concrete, Struct. Eng. Mech. 80 (2) (2021) 181–199.
[95] B.A. Tayeh, A.M. Zeyad, I.S. Agwa, M. Amin, Effect of elevated temperatures on mechanical properties of lightweight geopolymer concrete, Case Stud. Constr. Mater. 15 (2021), e00673.
[96] A. Demir, İ.B. Topçu, H. Kuşan, Modeling of some properties of the crushed tile concretes exposed to elevated temperatures, Constr. Build. Mater. 25 (4) (2011) 1883–1889.
[97] J. Eidan, I. Rasoolan, A. Rezaeian, D. Poorveis, Residual mechanical properties of polypropylene fiber-reinforced concrete after heating, Constr. Build. Mater. 198 (2019) 195–206.
[98] M.A. Sherif, Effect of elevated temperature on mechanical properties of nano materials concrete, Int. J. Eng. Innov. Technol. 7 (2017) 1–9.
[99] I.Y. Hakeem, M. Amin, B.A. Abdelsalam, B.A. Tayeh, F. Althoey, I.S. Agwa, Effects of nano-silica and micro-steel fiber on the engineering properties of ultra-high performance concrete, Struct. Eng. Mech. 82 (3) (2022) 295–312.
[100] G.A. Rao, Investigations on the performance of silica fume-incorporated cement pastes and mortars, Cem. Concr. Res. 33 (11) (2003) 1765–1770.
[101] H. Vikan, H. Justnes, Rheology of cementitious paste with silica fume or limestone, Cem. Concr. Res. 37 (11) (2007) 1512–1517.
[102] Z. Wu, C. Shi, K.H. Khayat, Influence of silica fume content on microstructure development and bond to steel fiber in ultra-high strength cement-based materials (UHSC), Cem. Concr. Compos. 71 (2016) 97–109.